Smart Structures and Systems, Vol. 1, No. 4 (2005) 369-384
DOI: http://dx.doi.org/10.12989/sss.2005.1.4.369

Embedded smart GFRP reinforcements for monitoring reinforced concrete flexural components

Anastasis V. Georgiades†, Gobinda C. Saha‡, Alexander L. Kalamkarov‡‡ and Srujan K. Rokkam‡†

Mechanical Engineering Department, Dalhousie University, Halifax, NS B3J 2X4, Canada

John P. Newhook‡‡†

Civil Engineering Department, Dalhousie University, Halifax, NS B3H 3J5, Canada

Krishna S. Challagulla‡‡‡

Mechanical Engineering Department, Dalhousie University, Halifax, NS B3J 2X4, Canada

(Received May 24, 2005, Accepted September 20, 2005)

Abstract. The main objectives of this paper are to demonstrate the feasibility of using newly developed smart GFRP reinforcements to effectively monitor reinforced concrete beams subjected to flexural and creep loads, and to develop non-linear numerical models to predict the behavior of these beams. The smart glass fiber-reinforced polymer (GFRP) rebars are fabricated using a modified pultrusion process, which allows the simultaneous embeddement of Fabry-Perot fiber-optic sensors within them. Two beams are subjected to static and repeated loads (until failure), and a third one is under long-term investigation for assessment of its creep behavior. The accuracy and reliability of the strain readings from the embedded sensors are verified by comparison with corresponding readings from surface attached electrical strain gages. Nonlinear finite element modeling of the smart concrete beams is subsequently performed. These models are shown to be effective in predicting various parameters of interest such as crack patterns, failure loads, strains and stresses. The strain values computed by these numerical models agree well with corresponding readings from the embedded fiber-optic sensors.

Keywords: smart GFRP rebar; Fabry-Perot sensors; structural strain and deformation; creep; finite element modeling.

1. Introduction

Interest in composite materials has led in recent years to their integration within such areas as the aerospace industry, civil engineering, transportation and marine engineering. At the same time,

†Assistant Professor, E-mail: Georgiades@dal.ca
‡Post-doctoral Fellow, E-mail: Gsaha@dal.ca
‡†Professor, Director, Corresponding Author, E-mail :Alex.Kalamkarov@dal.ca
‡‡MASc. candidate, E-mail: SRokkam@dal.ca
‡‡†Associate Professor, E-mail: John.Newhook@dal.ca
‡‡‡PhD candidate, E-mail: Kchallag@dal.ca

significant advancements in MEMS, telecommunications and other fields, significantly facilitated the development of new and highly effective sensors and actuators. It would thus seem natural that the ever-expanding field of composite materials would seek ways to take advantage of and encompass these advancements in actuator and sensor technology. The merge of these domains gave birth to the so-called “smart composite materials”. Smart composite materials are adaptive composite structures, which incorporate sensors and actuators. Depending on their type, smart composites can be classified as passive or actively controlled. Passive smart materials incorporate sensors that provide information on their state and integrity, while the actively controlled smart materials incorporate both sensors and actuators and they can perform self-adjustment or self-repair as conditions change.

Popular among strain-sensing devices, particularly for structural engineering applications, are fiber optic sensors (Feng, *et al.* 1995, Kim, *et al.* 1997, DeMerchant, *et al.* 2000, Tennyson, *et al.* 2000, 2001). These sensors have many advantages over traditional strain gages including resistance to EMI losses, inherent corrosion resistance, minimal need for cabling, a very small size which implies little or no disturbance to the structure being monitored, and the ability to make absolute strain measurements. A popular type of fiber optic gages is currently the Fabry-Perot fiber-optic sensor (FP-FOS) which is the sensor used in the present study.

The present research is part of the continuous effort to advance long-term non-destructive structural health monitoring systems for civil infrastructure. The study uses custom-built GFRP rebars with embedded FP-FOS sensors (Kalamkarov, *et al.* 1999, 2000a, 2000b, 2000c, 2004, 2005); these rebars are subsequently embedded in laboratory-fabricated reinforced concrete beams which are subjected to static and repeated loads (to failure) as well as to sustained loads for evaluation of their creep behavior. The ability of the embedded sensors to accurately monitor the strain state of a structure during service is assessed by comparing with other traditional devices such as electrical strain gages (ESG), and LVDT’s. Since the FP-FOS are embedded (rather than surface attached), they are afforded a higher degree of protection by the host composite rebar. This, in conjunction with the fact that the smart rebars can be produced efficiently and expediently by standard manufacturing techniques such as pultrusion, make the GFRP rebars a worthy tool in the design and assessment of concrete structures for an extended period.

The second major objective of the present study is the development of non-linear finite element (FE) models pertaining to the reinforced concrete beams with the smart rebars. The FE models are created using the ANSYS™ program. An eight-node solid element, SOLID65, capable of cracking in tension and crushing in compression is used to model the reinforced beams. The smart GFRP and steel rebars are modeled using the ‘smeared’ reinforcement approach of the SOLID65 element. The results obtained from the numerical analysis are compared to their experimental counterparts.

Following this introduction, the pultrusion, processing and reliability assessment of the smart GFRP tendons with the embedded FP-FOS sensors are discussed in Section 2. Section 3 gives the details on the fabrication of smart concrete beams as well as the comprehensive testing program to which the smart beams are subjected to. Section 4 gives the results of the experimental program and compares the health monitoring capabilities of the embedded FPFOS with electrical strain gages. In Section 5, the finite element modeling of the smart beams is carried out. The results obtained from this numerical approach are discussed and compared with their experimental counterparts in Section 6. Finally, Section 7 concludes the paper.

2. Background

2.1. Fabry-Perot fiber-optic sensors

In this study, the fiber-optic sensors that are embedded during the pultrusion of GFRP tendons are of the Fabry-Perot type with a $\pm 3000\ \mu\varepsilon$ capability. The sensors are acquired as prepackaged assemblies (0.01% of full scale resolution) and are non-compensated for thermal strains (RocTest 2000). The Fabry-Perot sensor has been developed to use a broadband light source as opposed to laser light. It is highly sensitive and can make precise, linear and absolute measurements (Kalamkarov, *et al*. 1999).

2.2. Fabrication and assessment of smart pultruded GFRP rebar with embedded FP-FOS

The concrete beams used in the present study use GFRP rods with embedded FP-FOS for structural monitoring purposes. The pultruded GFRP rods (Ø9.5 mm) are produced using a urethane-modified bisphenol-A based vinyl ester resin system known for its good mechanical properties and excellent processability (Kalamkarov, *et al*. 1999, 2000a). Two types of organic peroxide catalysts are used to cure the resin: di-peroxydicarbonate and tert-butyl peroxybenzoate. Adequate release from the die is achieved using an internal lubricant. The pultrusion process is modified in order to allow the embeddement of Fabry-Perot sensors within the pultruded composite rods (Kalamkarov, *et al*. 1999, 2000a). To comprehensively examine the behavior of the pultruded sensor, the GFRP rods were previously subjected to quasi-static sinusoidal and trapezoidal load waveforms under conditions of high (up to +60°C) and low (up to -40°C) temperatures (Kalamkarov, *et al*. 2000b, 2000c). The reliability assessment of the fiber optic sensors further entailed the study of their fatigue and creep behavior as well as their performance when the rods in which they are embedded are placed in severe environments (e.g. alkaline solutions), which may simulate conditions encountered in concrete structures wherein the composite rods may be used as prestressing tendons or rebars. The results from these experiments (Kalamkarov, *et al*. 2000b, 2000c) showed an excellent agreement between the readings from the embedded FP-FOS and the corresponding ESG, extensometer, and/or theoretical values. The sensors retained their accuracy and repeatability throughout the tests, thus demonstrating a great potential for health monitoring of civil engineering infrastructures.

The next logical step is the investigation of the performance of the GFRP reinforcements with the embedded sensors in flexural members such as concrete beams. We would like to primarily assess the sensing capability of the embedded sensors. If it can be established that these small diameter smart GFRP rods are effective in structural health monitoring, then, by extension, larger diameter smart rebars can be used as both sensors and reinforcements thus creating a smart GFRP-reinforced concrete structure. To the best of the authors' knowledge, the health monitoring of concrete structures by virtue of sensors embedded within GFRP reinforcements has not been done before.

2.3. Surface treatment of GFRP rebars and setting up of strain gages

The interface between the smart tendon and the host concrete material is of paramount importance in achieving an effective strain transfer between the host material and the embedded sensor. However, the pultruded GFRP rods have a smooth surface which would make them susceptible to interfacial slip. To avoid this, a Ø1 mm silica sand epoxy coating is used to roughen their surface.

As mentioned earlier, the strain readings from the embedded FP-FOS will be compared with those from traditional electrical strain gages (ESG's). The precision strain gages used in this study are of CEA-13-125UW-350 type which are capable of forming a good bond with the GFRP surface. The ESG's are bonded onto a groove etched on the rod's surface, which also serves to protect them from accidental damage during handling, poring of the concrete etc. Once the gages are securely bonded, a three-layer protection scheme consisting of butyl rubber, electrical tape, and aluminum foil, is used to shield the gages and associated terminals against re-ionizing and detachment from the GFRP surface. It is evident that the overall bonding/protection scheme for the surface attached ESG's is rather cumbersome and time consuming and compares unfavorably with the quick and automatic methodology of pultruding the FP-FOS in the GFRP rebars.

3. Experimental program

3.1. Beam design specimens and materials

The performance of the GFRP rods with the FP-FOS will be assessed by means of an experimental program performed on concrete beams in which the smart rods are embedded. For this purpose, three

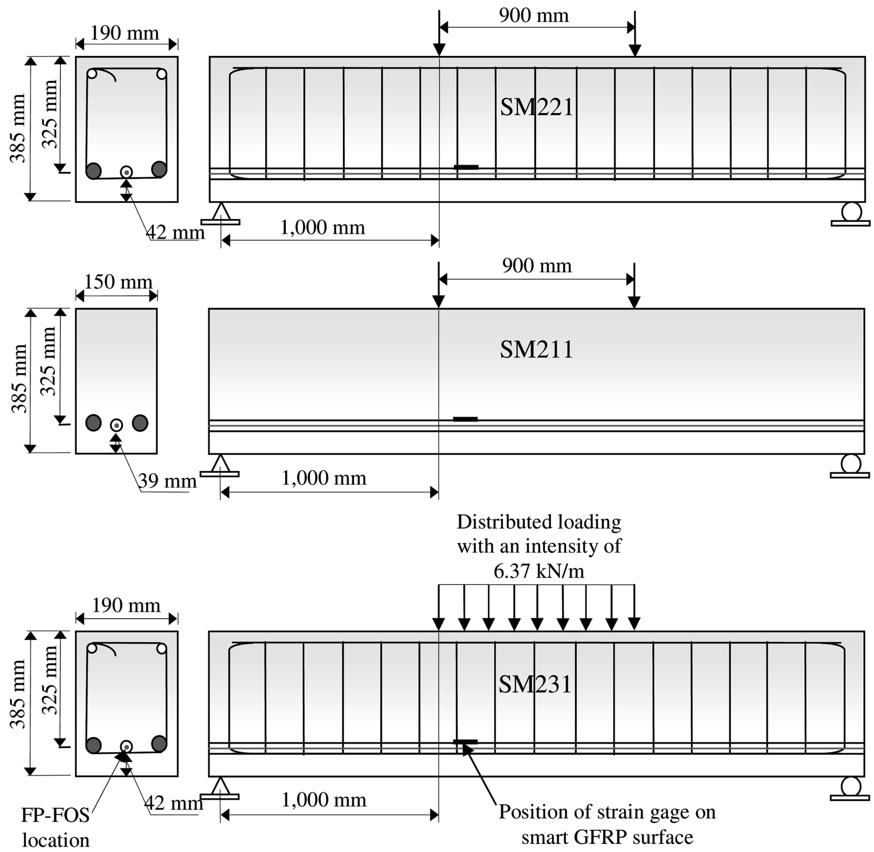

Fig. 1 Smart concrete beams and loading configurations

different beam designs are investigated. Two of these beams, SM221 and SM231 are shear-reinforced and the third, SM211 is of diagonal-tension type. The stirrups in beams SM221 and SM231 are made from Ø6 mm steel. The pertinent construction details are given in Fig. 1. ESG's are mounted on the surface of the GFRP rods near the location of the embedded sensors.

The concrete used for this study is a normal weight ready-mix type. The mixing proportions for a cubic meter of concrete include 340 kg Type-I cement, 1022 kg aggregate passing through a maximum sieve size of 25 mm, 880 kg sand, 170 kg water, and 0.8 kg MBL82 Water Reducer. The measured concrete compressive strength and modulus of elasticity from concrete cylinder tests are 34.3 MPa and 26.3 GPa, respectively. Beams are 60-day old at the time of testing.

The flexural capacity of the concrete beams is satisfied by using 25M steel rebars. The beams conform to CSA Standards A23.1 and G30.18 (1995). Beams SM211 and SM221 are subjected to static and repeated loads until failure, while beam SM231 is under long-term creep loading, with a distributed load configuration of 6.37 kN/m and a load span of 1.0 m (centralized), see Fig. 1. The dynamic strain outputs from the experiments are acquired through a DMI fiber-optic multi-channel field datalogger. LVDT's and high-precision dial indicators are used to measure the deflection at the desired locations.

3.2. Experimental setup and equipment

Two data acquisition systems are used: the DMI fiber-optic multi-channel field datalogger system for continuous strain and temperature monitoring from the FP-FOS and the Wheatstone Quarter Bridge Circuit Module P-3500 and Operational Amplifier Switch-And-Balance Unit SB-10 for monitoring the strain gages. The electrical resistance system is linear and varies between 0 and 400 mV with a sensitivity of 1.9 $\mu\varepsilon$/mV. In addition to the DMI system, a FIZ 10 demodulation unit (RocTest 2000) is used to dynamically read isolated strain values from the FP-FOS without interrupting the main DAQ program. LVDT's are used for deflection measurements. A schematic of the overall setup pertaining to beams SM211 and SM221 is shown in Fig. 2. A custom-made 1400 kN load frame with a 50T

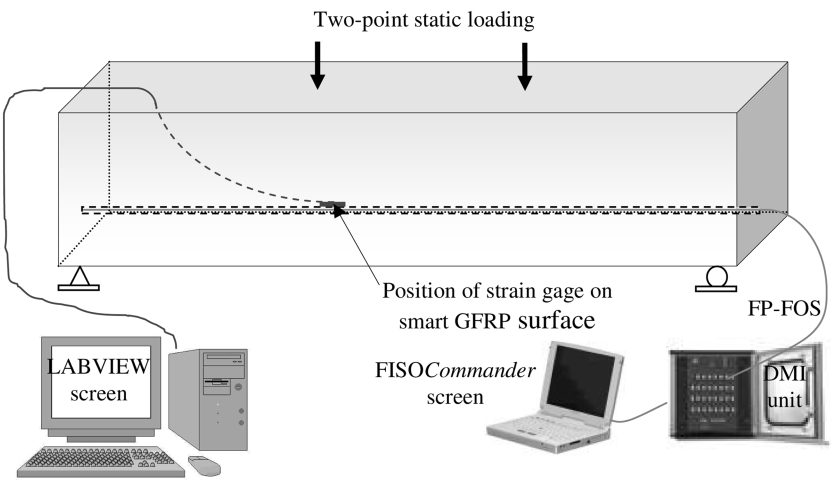

Fig. 2 Schematic of beam setup with data acquisition units

Fig. 3 Equipment setup just prior to testing of beam SM221

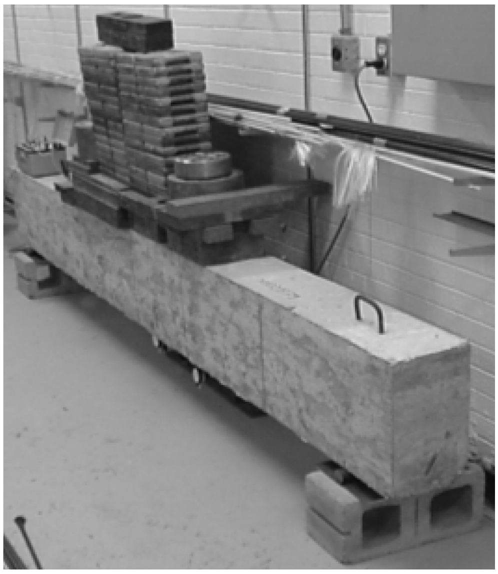

Fig. 4 Experimental setup for beam SM231 under creep loading

hydraulic jack system is used to load beams SM211 and SM221. Fig. 3 shows a photograph of the equipment setup just prior to testing of beam SM221.

The potential for use of embedded fiber-optic sensors in the assessment of long-term structural health by monitoring of creep strains is further investigated through testing of beam SM231. This beam is subjected to a distributed load of 6.37 kN/m with a load span of 1.0 m. A test setup for the beam is shown in Fig. 4. The temperature in the laboratory during the testing phase (175 days) varied from +6°C to +28°C. The average relative humidity over this period was about 60%.

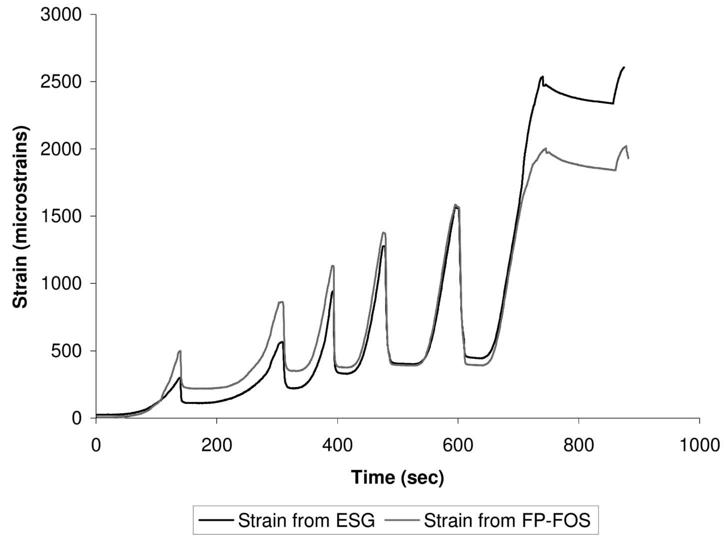

Fig. 5 Comparison of strain readings from FP-FOS and ESG for beam SM221

4. Experimental results and discussion

4.1. Beams SM211 and SM221

One of the primary objectives of this study is to assess how reliably the FP-FOS can read strain near and during concrete failure, and determine whether there are any significant advantages to using embedded sensors rather than, say, surface-attached strain gages. Theoretically, the sensor should continue to provide accurate data unless the GFRP rebar in which it is embedded ruptures causing debonding of the sensor, or unless a complete fracture of the sensor occurs due to shear and axial forces.

Static two-point load tests are conducted on beams SM211 and SM221. Since a load-controlled test is used instead of a displacement-controlled one, the specimens are loaded at a very slow rate to gather as many data points near failure as possible. At the end of each step, the loading, midspan deflection, deformation, strain output, and concrete crack patterns are recorded. The beams are simultaneously subjected to several loading-unloading cycles for the purpose of understanding residual deflection and strain accumulation behavior.

The static two-point loading tests on beams SM211 and SM221 reveal that both beams exhibit shear failure. As load increases with repeated cyclic loadings, shear stresses begin to dominate, increasing the number and density of cracks. The diagonal-tension crack is the cause for ultimate failure of the beams. More details on the failure of the beams are given in Section 6. Fig. 5 shows a comparison of the strain readings from the FP-FOS system and the ESG unit during this repeated loading on beam SM221. After an initial transient period, it is apparent that the strain readings of the FP-FOS agree well with their counterparts from the conventional ESG. The observed discrepancy at the failure load could possibly have been caused by a crack forming at the location of the ESG. Unlike the surface-attached ESG, the fiber-optic sensor would not have been affected by this crack because it is embedded into (and therefore protected by) the GFRP bar. This is a distinct advantage of embedded fiberoptic sensors. In fact, it is observed in these experiments that at, or near beam failure, the ESG's fail, whereas the

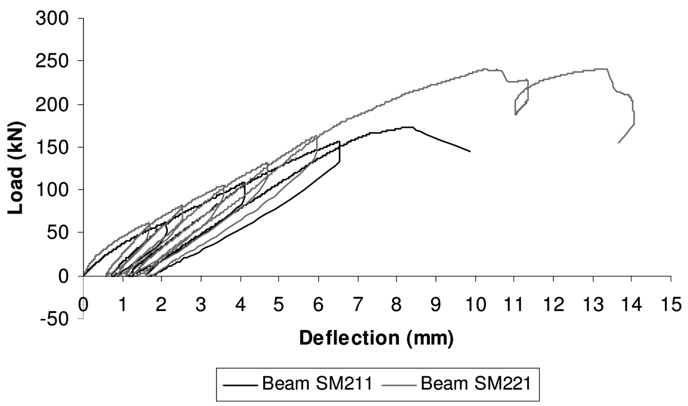

Fig. 6 Average deflection curves at the mid span of the beams SM211 and SM221

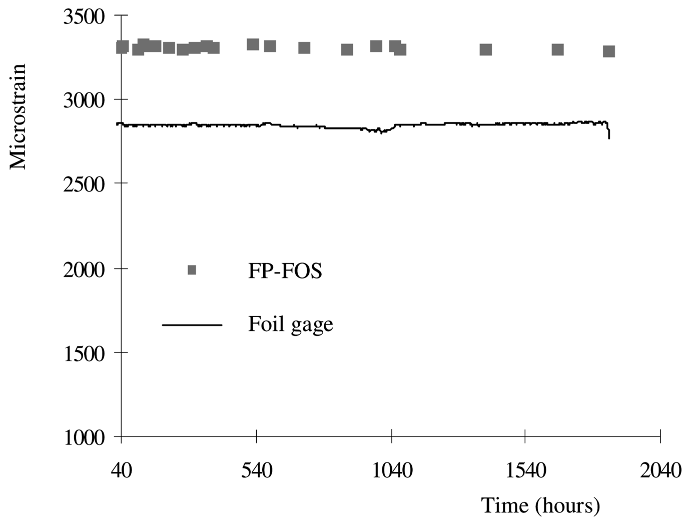

Fig. 7 GFRP rod with embedded FP-FOS in alkaline solution (pH. 12.8) with sustained load of 11 kN

embedded FP-FOS are still functioning reliably. The average deflection curves at the midspan of beams SM221 and SM211 are shown in Fig. 6. More details on the experiments and results pertaining to these two beams can be found in Kalamkarov, *et al.* (2005).

Further discussion on the performance of the fiber-optic sensors is given in Section 6, when the experimental results are compared with finite element based numerical analysis.

4.2. Beam SM231

The main objective of the testing performed on beam SM231 is to further investigate the long-term structural health-monitoring capability of embedded fiber-optic sensors through the monitoring of creep strains. Previous research conducted on the smart GFRP rods alone (Kalamkarov, *et al.* 2000b, 2000c) has demonstrated the ability of the embedded FP-FOS to monitor creep strain, see Fig. 7. Thus, it would be of interest to extend these tests and assess the behavior of the sensors when embedded in concrete structures.

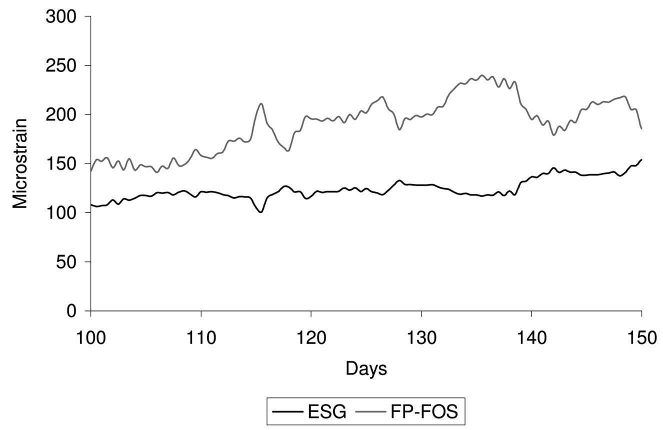

Fig. 8 Beam SM231: strain vs. time from ESG and FP-FOS

Table 1 Thermal strain of strain monitoring devices

Devices with location	CTE (με /^{o}C)
LVDT affixed externally (on concrete)	10
FP-FOS embedded in smart GFRP	8.9
ESG mounted on smart GFRP surface	0.6

As mentioned in Section 3.2, beam SM231 was subjected to a sustained 6.37 kN/m distributed load with a load span of 1.0 m. Fig. 8 compares the strain readings from the FPFOS and the ESG. In the 3-5 month period, the two strain-monitoring devices do not record significant creep strains. The discrepancy between the two devices is likely to have been caused by the fact that the FP-FOS and the ESG are not at the same locations along the span of the beam. During these experiments, high-precision dial indicators are used to measure the beam deflection at mid span and at the location of the embedded sensor.

Before closing this section, it should be mentioned that the FP-FOS's used in the present study cannot distinguish between thermal and mechanical strains. It is however desirable to isolate the mechanical strain from its thermal counterpart. Hence, in the experiments discussed in this paper, the thermal strain is factored out of the readings of each strain monitoring device (FP-FOS, or ESG) and the details are given in Table 1. Thus, the mechanical strain is computed as:

$$\varepsilon = \varepsilon_m - \varepsilon_{th} \tag{1}$$

where ε_m and ε_{th} are the measured (total) and thermal strains pertaining to each strain-monitoring device, respectively.

5. Finite element modeling of reinforced concrete beams

5.1. Background

Although empirical methods remain adequate for ordinary design of reinforced concrete sections,

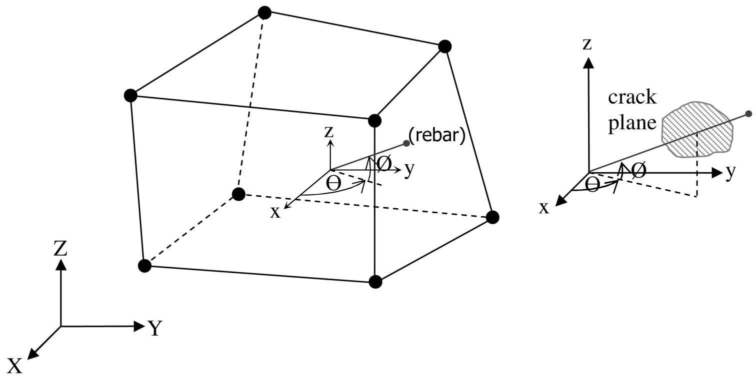

Fig. 9 SOLID65 element geometry and stress output

numerical techniques such as the finite element method (FEM) provide a better means of analysis of more complex systems (Fanning 2001). A commonly used FE program, ANSYS, employs a model that allows the prediction of failure of brittle materials such as GFRP rebars embedded in a host material like concrete (Matthews, *et al.* 2000, ANSYS 2004). It also allows the investigation of plastic deformation and creep in the host material as well as in the embedded (reinforcing) rebars.

The numerical model examined in this paper is stress/strain based, and it incorporates critical energy release and damage mechanics. It is assumed that crack initiation depends on a critical stress value and crack propagation depends upon released energy values. The main challenge here however is the combination of stresses pertinent to a multiaxial stress state, with interactions between the different elements within the reinforced beam. To this end, we choose element SOLID65, which employs the concept of 'smeared crack approach' (ANSYS 2004). Hence, if cracking occurs at an integration point, it is dealt with through an adjustment of material properties. Effectively, the cracks are treated as 'smeared bands', rather than discrete cracks (ANSYS 2004). As well, the reinforcement capability is considered to be 'smeared' throughout the element. This is achieved by replacing the volume of the reinforced sections of the beam with an equivalent volume of smeared reinforcements such that their direction and the volume ratio of rebars to concrete is maintained. Prediction of the nonlinear response of concrete is based on a constitutive model for triaxial behavior of concrete (William and Warnke 1974, ANSYS 2004).

Table 2 Material input data in FEM (SOLID65)

Concrete	Glass FRP	Steel
Elastic modulus, E_c=26.3 GPa	Elastic modulus in x-direction, Ex = 47.3 GPa	Elastic modulus, E_s=207 GPa
Ultimate uniaxial compressive strength, f_c' = 34.26 MPa		Yield stress, f_y = 295 MPa
Ultimate uniaxial tensile strength (modulus of rupture), f_r = 3.51 MPa	Poisson's ratio in major x-y plane, υ_{xy}=0.22	Poisson's ratio, υ = 0.30
Poisson's ratio, υ = 0.20 (under sustained load) Shear transfer coefficient, β_t = 0.208-0.32 (open crack) Shear transfer coefficient, β_c = 0.90-0.92 (closed crack)		

5.2. Element formulation based on ANSYS SOLID65

The element, shown in Fig. 9, is used for the 3-D modeling of reinforced concrete. The solid feature of this element (with both cracking and crushing capabilities) is used to model the concrete, while the rebar feature can be used to model a reinforcing rebar. The element has eight nodes each with three degrees of freedom; translation in the x, y, and z directions. Both steel and GFRP rebars are used. The orientation of the rebars is graphically verified with the /ESHAPE command (ANSYS 2004), and is defined by two angles, θ and Ø (in degrees), with respect to the elemental coordinate system. Rebar specifications, which are entered as real constants, include the volume ratio and the orientation angles. Concrete material data such as shear transfer coefficients, uniaxial (tensile) cracking stress, uniaxial and biaxial crushing stresses, etc. are used as inputs and are provided in Table 2. When an element is cracked or crushed, a small amount of stiffness is added to it for numerical stability. The KEYOPT(7) command is used to accelerate convergence of the calculations when cracking is imminent (ANSYS 2004). After the solution converges (to the cracked state), the stiffness normal to the crack face is set to zero.

5.3. Modeling of a crack

To simulate experimental conditions as closely as possible, a static analysis is used for the numerical model. Specific details regarding the modeling of a crack can be found in (ANSYS 2004). Briefly, the total load acting on the beam is applied in a series of load increments. At the end of each load increment, the principal stresses are computed at the integration points and evaluated on the basis of the William and Warnke (1974) failure criterion. If any of the principal stresses lie outside the pertinent failure envelope, then cracking is initiated. If a crack appears at an integration point, the stress-strain relationships are modified by introducing a plane of weakness perpendicular to the face of the crack. As well, the accompanying reduction in the ability to sustain sliding across the crack face is observed by means of a shear transfer coefficient, β_t. A parameter called "crack strain", ε_{ck}^{ck} (ANSYS 2004), is used to determine whether a crack at an integration point is open or closed. When a crack first appears at an integration point, it is assumed to be open for the next iteration. Subsequently, if the crack strain is negative, the crack is considered to be closed.

Otherwise, i.e., if $\varepsilon_{ck}^{ck} \geq 0$, the crack is assumed to be open (ANSYS 2004).

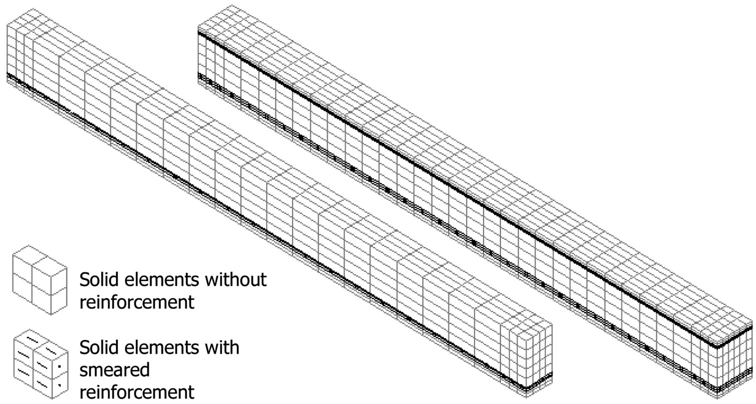

Fig. 10 Beams (SM211 & SM221): finite element mesh generation with smeared reinforcements: (a) in tension (b) in tension and compression

5.4. Mesh generation

For the problem at hand, a total discretization of the beam is generated and is shown in Fig. 10. For mesh generation, the model is composed of solid brick elements, the bottom portion of which contains the smeared reinforcements.

5.5. SOLID65 output data

The solution output associated with each element is in element nodal data. The output consists of the element derived data such as strains, stresses, and displacements. Due to the nonlinear nature of the analysis, the nodal solution is the value at the integration point closest to the node (ANSYS 2004).

6. FEM results, comparison with experimental data, and discussion

The main objectives of this part of the research are to investigate the suitability of the finite element model to analyze smart concrete beams with steel and GFRP reinforcements and verify its accuracy by comparison with pertinent experimental results (such as from FPFOS). The concrete cracking and crushing patterns as well as the load-strain and load-deflection responses for beams SM211 and SM221 are illustrated in Figs. 11-14. Figs. 11(a)-11(c) show the gradual development of cracks, in beam SM211, obtained by means of FE analysis, and Fig. 11(d) shows the experimental results for the said beam. Similar considerations apply to Figs. 13(a)-13(d), but they pertain to beam SM221. It is seen in Fig. 11(d) that the crack pattern in SM211 is in good agreement with its counterpart obtained through the FE

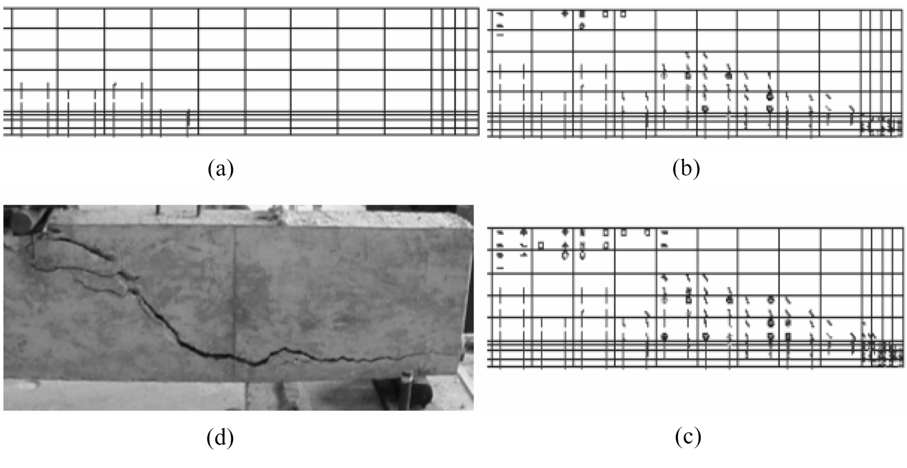

Fig. 11 Failure of beam SM211: experimental and FEM analysis

Table 3 Beam loadings from experiment and FE modeling

Beam identification	Ultimate load (experiment), kN	Final load (FEM), kN
SM211	173.1	174.5
SM221	241.0	246.0

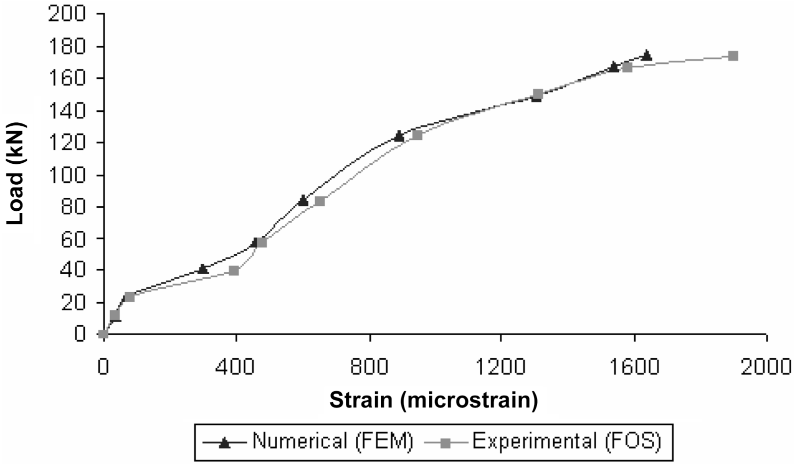

Fig. 12 Beam SM211: load vs. strain response from FP-FOS system and FEM analysis

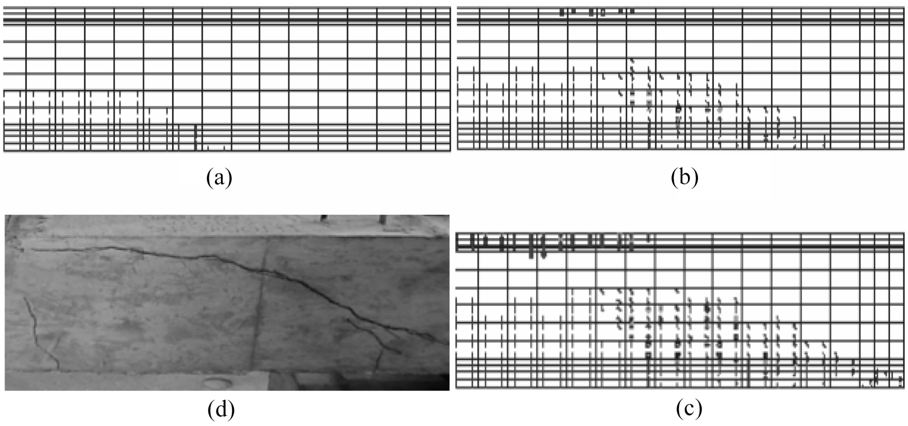

Fig. 13 Failure of beam SM221: experimental and FEM analysis

model and shown in Fig. 11(c). Enabling the 'crushing' capability of element SOLID65 (see Section 5) in the FE model causes this beam to fail in shear. The failure loads (see Table 3) pertaining to the experimental and numerical analysis are 173.1 kN and 174.5 kN, respectively, further evidence of the good degree of conformance between experiment and the numerical model. It should also be mentioned here that the convergence of the FE solution could not be achieved for shear transfer coefficients lower than 0.2 (closed crack) and 0.9 (open crack), see Table 2.

One of the main objectives of the current research is to assess the suitability of fiber-optic sensors, such as the FP type sensors embedded in GFRP rebars, to monitor the strain state of structures during service. To this end, Fig. 12 shows a comparison of the FE values with the experimental strain readings from the FP-FOS for beam SM211. It is evident that there is an excellent agreement between the two strain plots over the entire load range.

Similar observations can be made for the case of beam SM221. An inspection of Figs. 13(c) and 13(d) reveals that the crack pattern observed in this beam is similar to that obtained by the FE model.

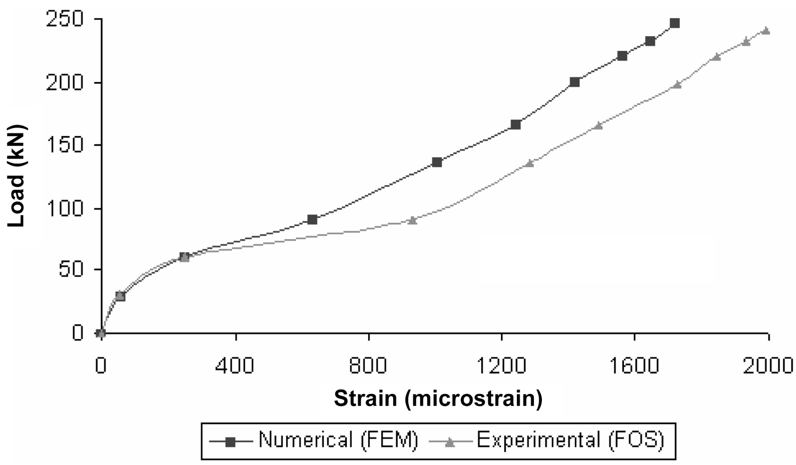

Fig. 14 Beam SM221: load vs. strain response from FP-FOS system and FEM analysis

Unlike beam SM211 (which exhibited sudden failure), beam SM221 is designed with stirrups in order to avoid catastrophic shear failure after the first crack. The primary motivation for this is to delay ultimate failure so that the FP sensor can provide strain data after first cracking. The failure loads (see Table 3) are 241 kN (experiment) and 246 kN (FE model). The shear transfer coefficients (see Table 2) used for convergence of the FE model are 0.32 (closed crack) and 0.92 (open crack). Fig. 14 shows a comparison of the FE values with the experimental (from embedded sensor) strain readings relevant to this beam. It is seen that for low load levels the FOS readings and the FE-based results agree very well with one another, but as we move into the nonlinear region they begin to show some discrepancy, although both strain plots exhibit similar trendline characteristics.

The results described in this paper are encouraging as to the potential of fiber-optic sensors to monitor the strain state of structures during service. If these sensors are embedded (rather than, say, surface attached) they are afforded a higher degree of protection by the host composite rebar; furthermore, the smart GFRP rebars can be produced efficiently and expediently by modifying a standard pultrusion process (Kalamkarov, *et al.* 1999, 2000). Since these small diameter smart GFRP rods are effective in structural health monitoring, then, by extension, larger diameter smart rebars can fulfill a dual role; reinforcing elements by virtue of their mechanical properties and strain monitoring devices by virtue of the embedded sensors.

7. Conclusions

A modified pultrusion process is used to successfully fabricate glass FRP rods with embedded fiber-optic sensors. These smart rods are embedded in three reinforced concrete beams. Two of these beams are subjected to static and repeated loads to failure, while the third one is under a long-term investigation for assessment of its creep behavior.

The experiments indicated a good degree of conformance between the FP-FOS embedded in the GFRP rebars and the EGS attached to the surface of the rebars. Thus, fiber-optic sensors can accurately monitor the strain state of a structure during service. Furthermore, since FP-FOS's are embedded (rather than surface attached) they are afforded a higher degree of protection by the host composite rebar. This, in conjunction with the fact that the smart rebars can be produced efficiently and expediently by standard manufacturing techniques such as pultrusion, make the GFRP rebars a worthy tool in the design, assessment and monitoring of concrete structures.

The performance of the smart concrete beams is further investigated by means of nonlinear FE models. FE modeling makes use of the SOLID65 element in ANSYS™. This element is capable of both cracking and crushing and is particularly suited to the analysis of reinforced concrete structures. This paper shows that the FE models are effective in predicting various parameters of interest, such as crack patterns, failure modes, ultimate loads, and strains and displacements. The strain values computed by the FE models agree well with corresponding readings from the embedded fiber-optic sensors.

In summary, this paper shows that element SOLID65 can be effectively used to model reinforced concrete structures. As well, FP-FOS embedded in GFRP rebars have excellent potential in structural health monitoring. Consequently, by extension, larger diameter smart rebars can be used as both sensors and reinforcements thus creating a smart GFRP-reinforced concrete structure.

Acknowledgements

The support by the Canadian Network of Centres of Excellence on the Intelligent Sensing for Innovative Structures (ISIS-Canada), the Natural Sciences and Engineering Research Council of Canada (NSERC), and the Killam Foundation is gratefully acknowledged.

References

ANSYS (2004), *ANSYS User's Manual Revision 8.1*, Canonsburg, PA.

Canadian Portland Cement Association (1995), *Concrete design handbook*, 2nd edn.

DeMerchant, M., Brown, A., Smith, J., Bao, X. and Bremner, T. (2000), "Distributed strain sensing for structural monitoring applications", *Canadian J. Civ. Eng.*, **27**, 873-879.

Fanning, P. (2001), "Nonlinear models of reinforced and post-tensioned concrete beams", *E. J. Struc. Eng.*, **2**, 111-119.

Feng, Q. M., Suzuki, H. and Yokoi, I. (1995), "Development of optical sensing systems for smart civil infrastructure", *Smart Mater. Struct.*, **4**, A114-A120.

Kalamkarov, A. L., Fitzgerald, S., MacDonald, D. and Georgiades, A. V. (1999), "On the processing and evaluation of pultruded smart composites", *Comp. Part B: Eng.*, **30B**(2), 167-175.

Kalamkarov, A. L., Georgiades, A. V., MacDonald, D. and Fitzgerald, S (2000a), "Pultruded fiber reinforced polymer reinforcements with embedded fiber optic sensors", *Canadian J. Civ. Eng.*, **27**, 972-984.

Kalamkarov, A. L., Fitzgerald, S., MacDonald, D. and Georgiades, A. V. (2000b), "Mechanical performance of pultruded composite rods with embedded fiber-optic sensors", *J. Comp. Sci. Tech.*, **60**, 1171-1179.

Kalamkarov, A. L., MacDonald, D., Fitzgerald, S. and Georgiades, A. V. (2000c), "Reliability assessment of pultruded FRP reinforcements with embedded fiber-optic sensors", *Comp. Struc.*, **50**, 69-78.

Kalamkarov, A. L., Saha, G. C., Georgiades, A. V., Challagulla, K. and Newhook, J. P. (2004), "Smart FRP reinforcements for long-term health monitoring in Infrastructure", *J. Thermoplastic Compo. Mater.*, **17**, 359-381.

Kalamkarov, A. L., Saha, G. C., Rokkam, S., Newhook, J. and Georgiades, A. V. (2005), "Strain and deformation monitoring in infrastructure using embedded smart FRP reinforcements", *Composites: Part B*, **36**, 455-467.

Kim, K. S., Ryu, J. U., Lee, S.J. and Choi, L. (1997), "In-situ monitoring of Sungsan bridge in Han river with an optical fiber sensor system", *SPIE*, **3043**, 72-76.

Matthews, F. L., Davies, G. A. O., Hitchings, D., and Soutis, C. (2000), *Finite Element Modeling of Composite Materials and Structures*, CRC Press, Boca Raton.
RocTest Ltd. (2000), *Instruction Manual: sensoptic fiber-optic sensors*, St-Lambert, QC, Canada.
Tennyson, R. C., Coroy, T., Duck, G., Manuelpillai, G., Mulvihill, P., Cooper, D. J. F., Smith, P. W. E., Mufti, A. A. and Jalali, S. J. (2000), "Fiber optic sensors in civil engineering structures", *Canadian J. Civ. Eng.*, **27**, 880-889.
Tennyson, R. C., Mufti, A. A., Rizkalla, S., Tadros, G. and Benmokrane, B. (2001), "Structural health monitoring of innovative bridges in Canada using fiber optic sensors", *Smart Mater. Struct.*, **10**, 560-573.
William, K. J. and Warnke, E. D. (1974), "Constitutive model for the triaxial behavior of concrete", *Int. Assoc. for Bridge and Structural Engineering*, **19**, 1-30.

CC